The 2019 World Congress on
Advances in Structural Engineering and Mechanics (ASEM19)
Jeju Island, Korea, September 17 - 21, 2019

Seismic response of bridge-subgrade-CRTS II track system of High-Speed Railway under pulse-like strong motions

Yulin Feng[1)], Lizhong Jiang[2)], *Wangbao Zhou[3)], Binbin He[4)] and Leixin Nie[5)]

[1), 2), 3), 5)]*School of Civil Engineering, Central South University, Changsha, 410075, China* ;[4)]*University of Chinese Academy of sciences, Beijing 100049, China*
[3)] zhouwangbao@163.com

ABSTRACT

Taking the integral system composed of High-Speed Railway continuous girder bridge, simply supported approach bridge, subgrade at both ends and CRTS II track (HSR-CSII) as an example, two HSR-CSII models were established based on FEM, 20 ground motions with or without pulse-like with the same seismic mechanism, surface rapture directivity, rupture velocity and other factors were selected as the input based on QuakeManager. The time history of displacement of brake pier, approach bridge pier's top and the maximum displacement of each layer of the system in the two HSR-CSII models were extracted for comparative verification; furthermore, the influence of pulse-like on the seismic response of HSR-CSII model was compared and analyzed. The results show that the two models agree well with each other, which verifies the validity of the model; under the excitation of transverse bridge, the maximum envelope of lateral displacement of each layer of the system tends to be consistent, and the response of each layer of the system under pulse-like ground motion is greater than that without pulse-like ground motion; the smaller the pulse-like period, the more obvious the amplification effect of the pulse-like effect on the HSR-CSII response.

Key words: railway; forward-directivity pulse; fling-step pulse; ballastless track

1. INTRODUCTION

As an important form of high-speed railway infrastructure, bridge structure has an average busy ratio of 53% in the existing high-speed railway lines, that means high-speed trains run most of the time on the bridge(Zhai *et al*. 2014, Gou *et al*. 2018, Jiang *et al*. 2019). However, since China is located at the intersection of the two major seismic zones around the Pacific Ocean and Eurasia, there are at least 495 seismic fault zones in China. It is inevitable that high-speed railway bridges will be adjacent to or cross over faults. Based on the perspective of earthquake prevention and disaster reduction, it is necessary to study the pulse effect of near fault ground motion on

---

[1),4),5)] Graduate Student.
[2),3)] Professor.

high-speed railway bridges(Shao *et al*. 2014). The near-fault ground motion contains the forward-directivity pulse effect, the fling-step pulse effect, and it has obvious characteristics e.g. long period and high amplitude. With the deepening understanding of fault rupture mechanism, the researchers have paid attention to the difference of structural response caused by two kinds of pulse-like ground motions, the negative response of pulse-like ground motion to long-period structures has been paid more and more attention (Zhang *et al*. 2017). However, the influence of pulse type on the structure of high-speed railway bridges is not well understood. Compared with highway bridges, high-speed railway bridges have thick piers, larger vertical and horizontal heights, and lower longitudinal reinforcement ratio, generally less than 1%. For high-speed railway bridges with low reinforcement and large axial force, the effect of near-field pulse effect is still unclear. A few researchers have studied the pulse effect in the direction of near fault and the elastic-plastic response of high-speed railway bridges under vertical earthquake action by taking high-speed railway multi-span simply supported girder bridges as the research object, and proposed suggestions based on the design level (Chen *et al*. 2013, 2016). However, considering the track systems, multi-span approach bridges and subgrade at both ends of high-speed railway continuous girder bridges are rarely discussed. Therefore, it is necessary to take the subgrade and track systems of high-speed continuous girder bridge as a large system, and study its response under the pulse effect ground motion.

In this paper, a large system consisting of multi-span approach bridges, subgrade and high-speed railway continuous girder bridges with CRTS II slab ballastless track structure is studied under the pulse effect ground motion in the high-intensity area, two HSR-CSII models are established based on FEM. Based on QuakeManager software, the Stochastic simulation method is adopted to select a total of 15 near fault ground motions with the forward-directivity pulse effect(FDP), fling-step pulse effect (FSP), and no pulse effect (NOP) ground motion. The displacement time history of the braking pier, approach bridge pier's top in the two HSR-CSII models were extracted for mutual verification, and then the influence of pulse-like ground motion on the seismic response of HSR-CSII was analyzed.

2 HSR-CSII SYSTEMS

2.1 HSR-CSII simulation modeling

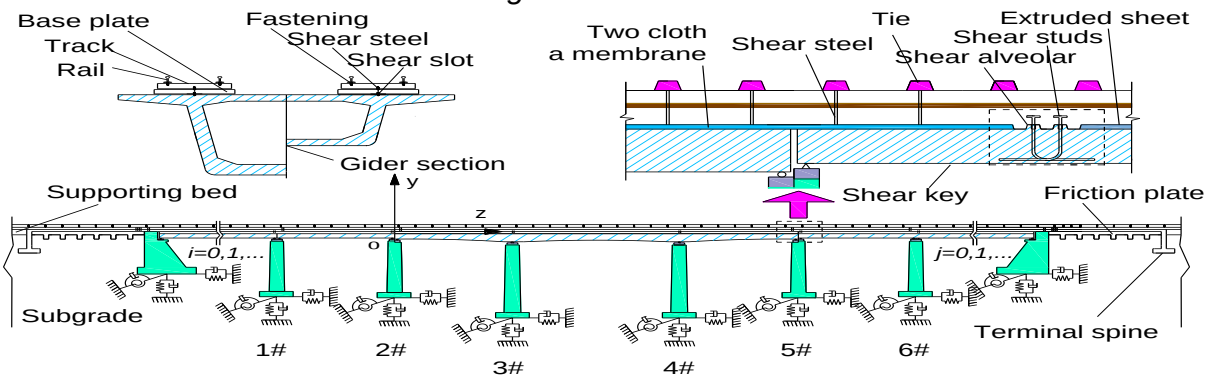

Fig.1 HSR-CSII simulation model

The main bridge of a high-speed railway bridge is (48+80+48) m a double continuous box girder bridge, the main girder adopts single box and single room section, variable height box girder, the girder height of mid-span section is 3.85m, the girder height of fulcrum section is 6.65m, the bottom of the girder is linearly graded with a quadratic parabola, the substructure is circular end solid pier, the approach bridges on both sides of the main bridge are 32m concrete simply supported box girder Bridges with single-box and single-room sections, as shown in Fig.1. The bearings are GQZs, as shown in Fig.2 (g). The key components of CRTS II slab ballastless track system include fastener, CA mortar layer, shear alveolar, shear steel, sliding layer, friction plate and so on (Kun *et al*. 2017), Combined with high-speed railway CRTS II plate ballastless track design principle(China Academy of Railway Sciences 2008) and existing research to determine the stiffness of key components(Li *et al*. 2018, Jiang *et al*. 2019).

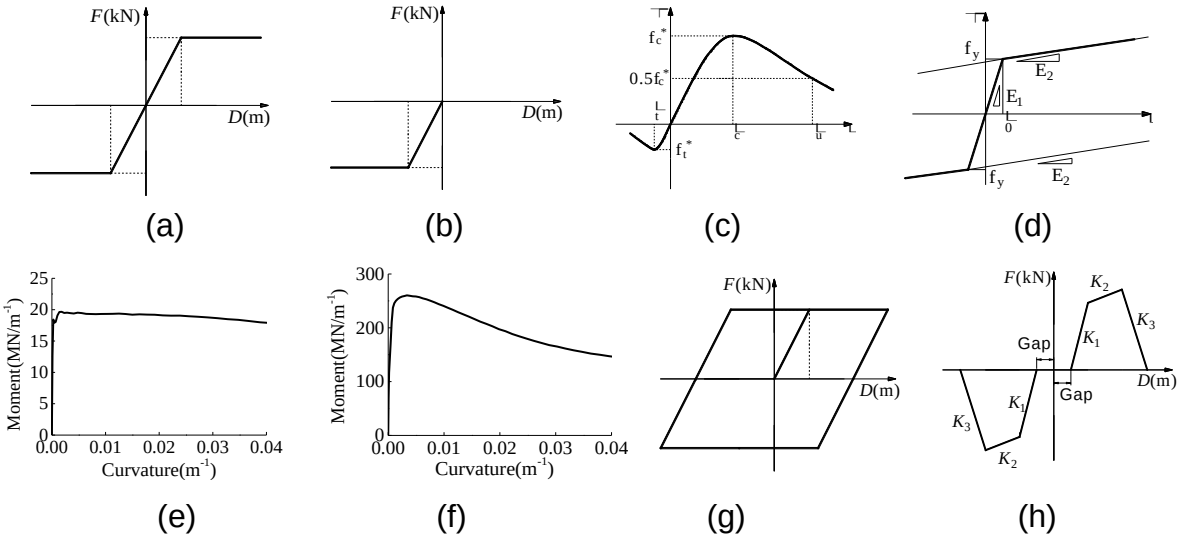

Fig. 2 (a)~(h) are ideal elastic-plastic constitutive model, only compression constitutive model, concrete and reinforcement constitutive model, Moment-curvature model of pier, bearing force-deformation and mechanical model of bearing limit block, respectively

2.2 Mechanism of simulation model

$$\begin{bmatrix} \mathrm{N} \\ \mathrm{M}_1 \\ \mathrm{M}_2 \\ \tau \\ \mathrm{S}_1 \\ \mathrm{S}_2 \end{bmatrix} = \begin{bmatrix} A_E(\varepsilon,\mathrm{T}) & & & & & \\ & \mathrm{I}_1^{\mathrm{E}}(\kappa_1,\mathrm{T}) & & 0 & & \\ & & \mathrm{I}_2^{\mathrm{E}}(\kappa_2,\mathrm{T}) & & & \\ & & & \mathrm{J}_{\mathrm{G}}(\chi,\mathrm{T}) & & \\ & 0 & & & \mathrm{A}_1^{\mathrm{G}}(\gamma_1,\mathrm{T}) & \\ & & & & & \mathrm{A}_2^{\mathrm{G}}(\gamma_2,\mathrm{T}) \end{bmatrix} \begin{bmatrix} \varepsilon \\ \kappa_1 \\ \kappa_2 \\ \chi \\ \gamma_1 \\ \gamma_2 \end{bmatrix} \quad (1)$$

Where, N and ε are axial force and axial strain, respectively; M_1, M_2 and κ_1, κ_2 are bending moment and curvature, respectively; τ, χ are torque, torsional ratio;

S_1, S_2 and γ_1, γ_2 are shear force and shear strain respectively; $A_E(\varepsilon,\mathrm{T})$, $I_1^{\mathrm{E}}(\kappa_1,T)$ and $I_2^{\mathrm{E}}(\kappa_2,T)$、 $J_{\mathrm{G}}(\chi,T)$, $A_1^{\mathrm{G}}(\gamma_1,T)$, $A_2^{\mathrm{G}}(\gamma_2,T)$ and T are the loudness of axial force, bending stiffness, torsional stiffness, shear stiffness and temperature, respectively.

Nonlinear beam element is used to simulate the key members between layers, The constitutive model of concrete tensile section (Fig.2 (c)) is adopted for concrete, and the double-broken line model is adopted for steel (Fig.2 (d)), The moment-curvature curve of pier is shown in Fig.2(e)~(f), and the mechanical model of bearing limit block (Fig.2(h)). The generalized beam element is constructed to simulate pier, the constitutive relation is shown as Eq(1). The effect of pile foundation is equivalent to six springs of pier bottom, and the stiffness of spring in six directions is used to simulate the effect of pile foundation (Sun *et al*. 2015) , the translational stiffness of the pile foundation in three directions is:

$$\gamma_{aaz} = \frac{n}{\dfrac{l_0+\xi h}{EA}+\dfrac{1}{C_0 A_0}} \tag{2}$$

$$\gamma_{aax} = \frac{n\delta_{MMx}}{\delta_{HHx}\delta_{MMx}-\delta_{MHx}^2} \tag{3}$$

$$\gamma_{aay} = \frac{n\delta_{MMy}}{\delta_{HHy}\delta_{MMy}-\delta_{MHy}^2} \tag{4}$$

The rotational stiffness of pile foundation in three directions is:

$$\gamma_{\beta\beta x} = \frac{n\delta_{HHx}}{\delta_{HHx}\delta_{MMx}-\delta_{MHx}^2}+\frac{\sum K_i x_i^2}{\dfrac{l_0+\xi h}{EA}+\dfrac{1}{C_0 A_0}} \tag{5}$$

$$\gamma_{\beta\beta y} = \frac{n\delta_{HHy}}{\delta_{HHy}\delta_{MMy}-\delta_{MHy}^2}+\frac{\sum K_i y_i^2}{\dfrac{l_0+\xi h}{EA}+\dfrac{1}{C_0 A_0}} \tag{6}$$

$$\gamma_{\beta\beta z} = \sum_i \sqrt{\frac{y_i^4}{\left(\delta_{HHx}^{(0)}\right)^2}+\frac{x_i^4}{\left(\delta_{HHy}^{(0)}\right)^2}} \tag{7}$$

Where, $\delta_{HHx}=\delta_{HHx}^{(0)}$, $\delta_{HHy}=\delta_{HHy}^{(0)}$, $\delta_{MHx}=\delta_{MHx}^{(0)}$, $\delta_{MHy}=\delta_{MHy}^{(0)}$, $\delta_{HMx}=\delta_{MHx}$, $\delta_{HMy}=\delta_{MHy}$, $\delta_{MMx}=\delta_{MMx}^{(0)}$, $\delta_{MMy}=\delta_{MMy}^{(0)}$ are the flexibility coefficients of each single pile; K_i is the number of roots installed in row i; n is the total number of roots of the pile; x_i, y_i are the distance from the origin of each pile to the axis of the pile, respectively; E is the elastic modulus of pile concrete, A is the average cross-sectional area of the pile into

soil; A_0 is the effective acting area of the base; ξ is the empirical coefficient; l_0, h are pile length of abovementioned part and soil penetration depth of pile below ground, respectively; C_0 is the vertical resistance coefficient of pile end foundation.

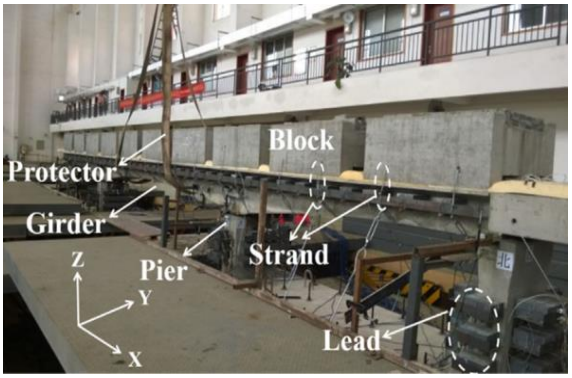

Fig. 3 HSR-CSII systems shaking table test

Table 1 Comparison of natural vibration characteristics of HSR-CSII

Order	Frequency/Hz	Period/s	Modal
1st	1.6268	0.6147	First-order symmetrical side bending of main girder
2nd	1.8353	0.5449	First-order longitudinal drift of main girder
3rd	1.8734	0.5338	First-order antisymmetric side bending of main girder
4th	1.9494	0.5130	Second-order symmetric side bending of main girder
5th	2.0144	0.4964	First-order symmetrical vertical bending of main girder
6th	2.4879	0.4019	Third-order longitudinal drift of main girder
7th	2.8217	0.3544	Third-order symmetrical side bending of main girder
8th	3.3184	0.3014	Second-order longitudinal drift of main girder
9th	3.3543	0.2981	Third-order longitudinal drift of main girder
10th	3.7417	0.2673	Third-order antisymmetric lateral bending of main girder

2.3 Simulation model validation

In order to verify the correctness of the simulation model in this paper, the shaking table test and finite element software verification were carried out, respectively. Based on the shaking table test and related research results of the three-span continuous girder bridge-single span approach bridge on both sides-CRTS II slab ballastless track system carried out by the research group in the early stage(Kang *et al*. 2017, Jiang *et al*. 2018, Gu *et al*. 2019), and the model is verified by shaking table test detailedly(Fig.3). The simulation model of this paper is expanded into a parametric simulation model of multi-span continuous girder bridge, multi-span approach bridge and subgrade on both sides and CRTS II type slab ballastless track system. Taking a seven-span HSR-CSII model as an example(Toyooka *et al*. 2005). The ANSYS and MIDAS are used to calculate the displacement time history of the brake pier, approach bridge pier's top displacement, and the comparison results are shown in Fig. 4.

It can be seen that the displacement time-history calculation results of the two models are in good agreement, indicating that the two numerical models are effective and can be used to analyze the seismic response of HSR-CSII system. Compared with MIDAS, ANSYS model can more conveniently analyze the influence of various influence parameters on the seismic response of the system, which can greatly shorten the modeling calculation time(Jiang *et al*. 2018, 2019). The following paper will use ANSYS numerical model for parameter analysis. Table 1 lists the characteristics of the first 10 modes and modes of HSR-CSII.

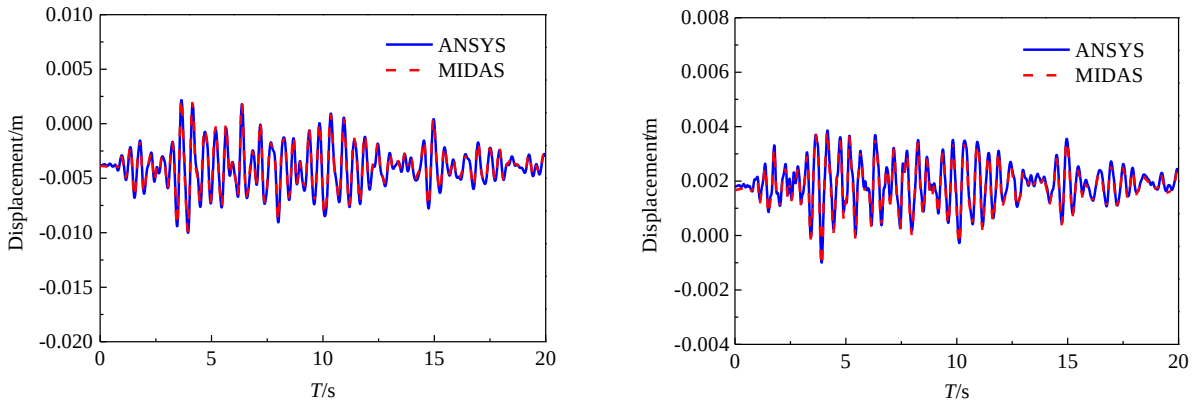

(a) (b)

Fig. 4 (a),(b)are the displacement time history of brake pier, approach bridge's top, respectively

3. GROUND MOTION SELECTION AND RESPONSE SPECTRUM ANALYSIS

Currently, the most common ground motion selected method is based on PEER NGA-west2. Although it can solve the problem of ground motion selection, there are many disadvantages. Firstly, the single fitting algorithm of the website program leads to a low fitting degree, and the selected average spectrum and target response spectrum have a large deviation; Secondly, site wave selection is always the priority to choose the common part of the seismic record, the operation will find that how to adjust the always used several times of the record, the latest earthquake records are difficult to fit. Thirdly, although the fitting degree of average spectrum and design spectrum is acceptable, the dispersion degree of the selected response spectrum of different ground motions is relatively large, and it is easy to see a large gap of structural response in the analysis. To sum up, the QuakeManager, a software based on ground motion database, adopts the Stochastic simulation method to select the ground motion at a height fitting to the target spectrum, the seismic database software has powerful wave selection parameter control functions, including all the seismic records of NGA and SAC. In order to avoid additional influences on the study due to different seismic mechanism, surface rupture form, rupture velocity and other factors, this study selected the same site category (Class C), compared and analyzed the seismic waves recorded by various stations in the same earthquake (Chi-Chi), A total of 15 ground motions are selected, including the FDP, FSP, and NOP. In the table2, the fault distance of near-fault ground motion is distributed discretely within 0~15 km, T_p is the impulse period, PGA、PGV、PGD

represent peak ground acceleration, velocity and displacement, respectively; PGV/PGA is the pulse parameter representing pulse effect.

Table 2. Ground motion grouping and its characteristic parameters

Earthquake	Station name	Fault distance /km	PGA/ (cm/s^2)	PGV / (cm/s)	PGV/PGA /s	T_p /s
FDP	TCU051	7.64	160.21	53.845	0.37	10.38
	TCU054	5.28	146.00	46.022	0.32	8.00
	TCU082	5.16	225.31	54.927	0.24	8.10
	TCU102	1.49	303.93	91.720	0.30	9.63
	TCU120	7.40	227.54	59.818	0.26	7.98
FSP	TCU052	0.66	357.55	151.207	0.43	11.96
	TCU052	0.66	446.91	172.335	0.39	11.96
	TCU068	0.32	511.68	249.594	0.49	12.29
	TCU068	0.32	370.91	264.065	0.72	12.29
	TCU075	0.89	331.98	109.554	0.33	4.99
NOP	TCU071	5.80	528.57	52.303	0.10	---
	TCU072	7.08	477.12	71.926	0.15	---
	TCU079	10.97	592.16	70.538	0.11	---
	TCU078	8.20	447.31	40.235	0.09	---
	TCU089	9.00	353.33	34.986	0.10	---

The spectral characteristics of three groups of ground motions were analyzed, after the ground motions of each group are normalized according to Table 2, according to the SeismoSignal software, PGA is uniformly adjusted to a design earthquake of 9 degrees (0.4g), and the elastic response spectrum and average spectrum of 5% damping ratio of linear elastic single degree of freedom under the action of ground motions of each group are calculated as shown in Fig.4.

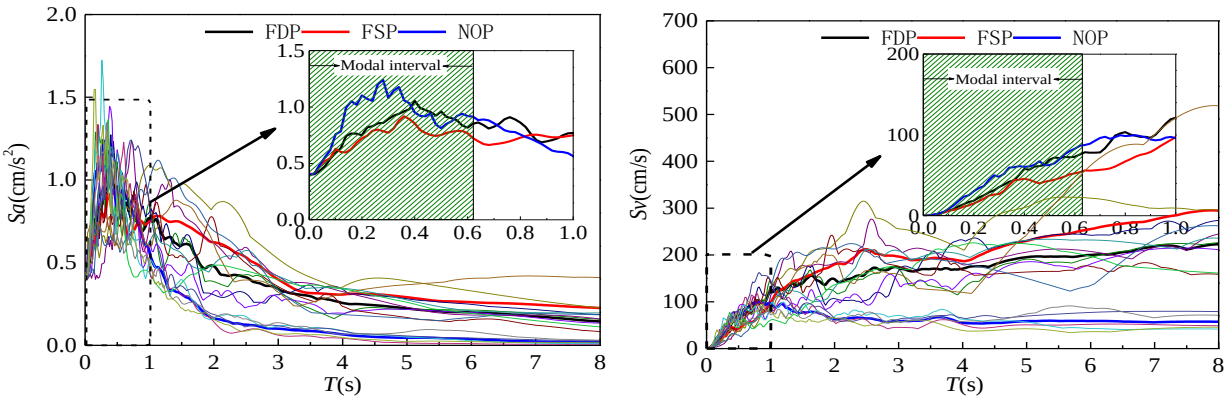

(a) Acceleration response spectrum (b) velocity response spectrum

Fig. 4 acceleration and velocity spectra of ground motions with different characteristics

Combined with Table 2 and Fig.4, it can be known that: For linear elastic single-DOF acceleration response spectrum, when the system period T<0.4s, the order of spectral acceleration average value is NOP>FDP>FSP; The corresponding period of peak acceleration of all types of ground motions is within the range of 0.3s~0.4s, and the peak acceleration of non-pulsed ground motions is higher than that of pulse-like ground motions; When the system period is 0.4s<T<1s, the spectral acceleration average value of the three groups of ground motions fluctuates up and down without obvious rule, when the system period T>1s, the tendency of spectral acceleration average value is FSP>FDP>NOP. For the linear elasticity velocity response spectrum, the law is the same as the acceleration response spectrum. The model interval of the selected HSR-CSII systems is within 0.62s, in the range of high frequency predominance period corresponding to the on-line elastic single-DOF acceleration response spectrum, therefore, the response law of the system under three groups of ground motions is random, different from the long-period structures maintain the characteristics of universal law of the seismic response.

3. HSR-CSII SYSTEM SEISMIC ANALYSIS UNDER PULSE-LIKE GROUND MOTION

In order to analyze the impact of pulse-like ground motion on HSR-CSII seismic response, the ground motion records in Table 2 are input into the above HSR-CSII model, respectively. Take the peak displacement of each layer of the system as the sampling point; the peak displacement of rail (D_r) , the peak displacement of track plate (D_t) , Peak displacement of base plate (D_p) , Peak displacement of main girder (D_b) as the sampling points, Xr is mileage.

3.1 The influences of pulse effect

Figs. 5~6 show that, the seismic response characteristics of rail, track, base plate and main girder are basically the same under three groups of ground motions, but the response amplitude is obviously different, this is because HSR-CSII is a short period rigid structure, from the linear elasticity response spectrum with single-DOF, it can be found that the response spectrum values of the three groups of ground motions vary intricately in the high frequency range of 0~1s, resulting in different mode orders of motivated HSR-CSII, so the HSR-CSII response is different.

Under the excitation of the transverse bridge direction, the envelope diagram of lateral displacement of each layer under the three groups of ground motions tends to be consistent and the values are basically close, mainly because the lateral block of lateral limit set on the bridge restricts the displacement of the track system. The system response of the FDP is the largest, followed by the FSP, and the NOP is the lowest; The influence of the FDP (FSP) on the maximum lateral displacement of each layer is 82.81%(63.14%), 82.98%(63.32%), 83.35%(64.12%), 79.15%(59.99%), successively. Lateral displacement peaks appear along the length of each layer in girder joints, and it reaches the maximum value in the span of continuous girder, the rail, track of subgrade and friction plate section and base plate of friction plate section did not appear transverse deformation.

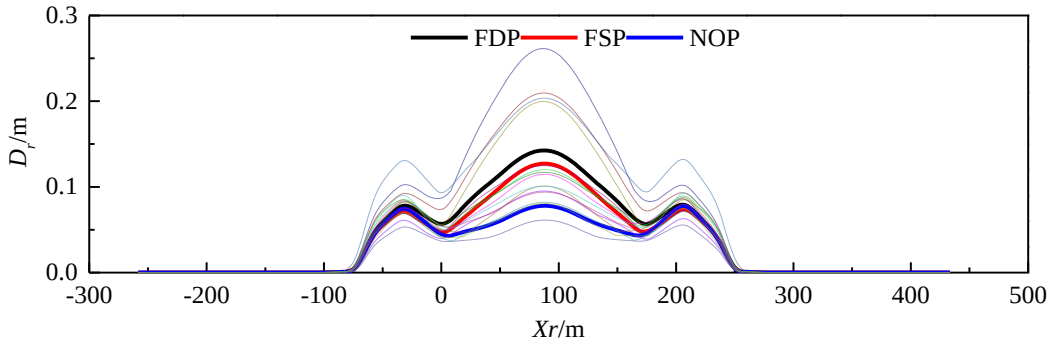

(a) Displacement envelope diagram of rail

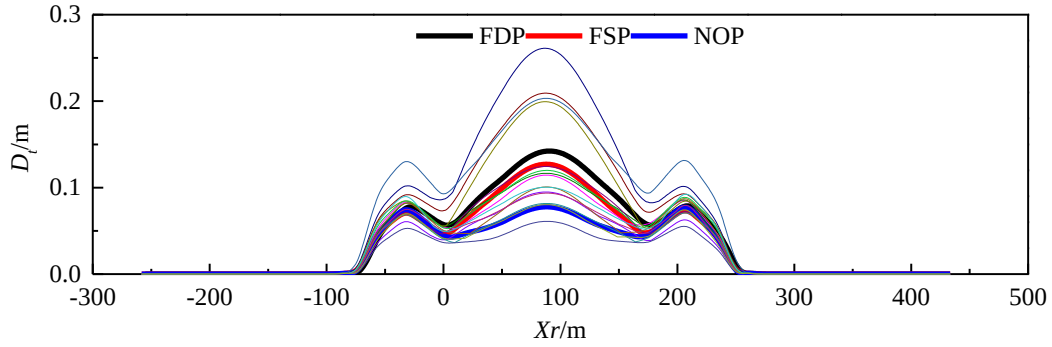

(b)Displacement envelope diagram of track

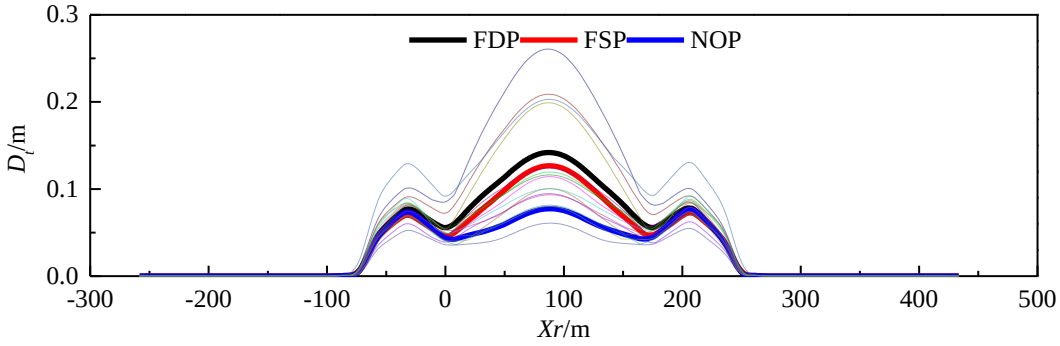

(c) Displacement envelope diagram of base plate

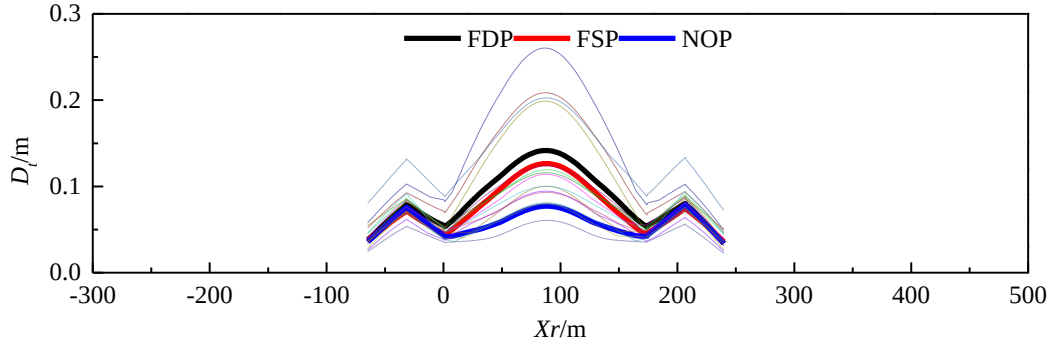

(d) Displacement envelope diagram of main girder

Fig. 6 The average lateral displacement envelope diagram of each layer under the three groups of ground motions

3.2. The influences of PGV/PGA

As can be seen in Figs.7-8, with the increase of PGV/PGA value, the maximum transverse displacement of rail, track, base plate and main girder under the three groups of ground motions tends to increase, the main reason is that the ground motion with a small value of PGV/PGA contains more high-frequency components, the loading and unloading speed is fast, the inertial force acting in the same direction on each layer does not last long, and the response of the structure does not have enough time to accumulate, therefore, the seismic response of each layer under the action of the ground motions with a small PGV/PGA value is smaller, for ground motions with a large PGV/PGA value, seismic energy is distributed in the low-frequency region, the loading and unloading speed is slow to transform, and the acceleration pulse that maintains in the same direction lasts for a long time. After the deformation of each layer, there is enough energy to continue to produce larger displacement in the sliding direction of each layer, so the response is large. In particular, the reason why the response of each layer under the FSP ground motion shows a decreasing trend may be that the FSP ground motion at this time just motives a certain mode of vibration of the system and forms resonance with the frequency band contained in the ground motion. By observing the scatter trend, it can be found that, with the increase of PGV/PGA, the dynamic response value rises sharply under the NOP ground motion, however, the dynamic response value presented a moderate growth trend under the action of the FDP and FSP.

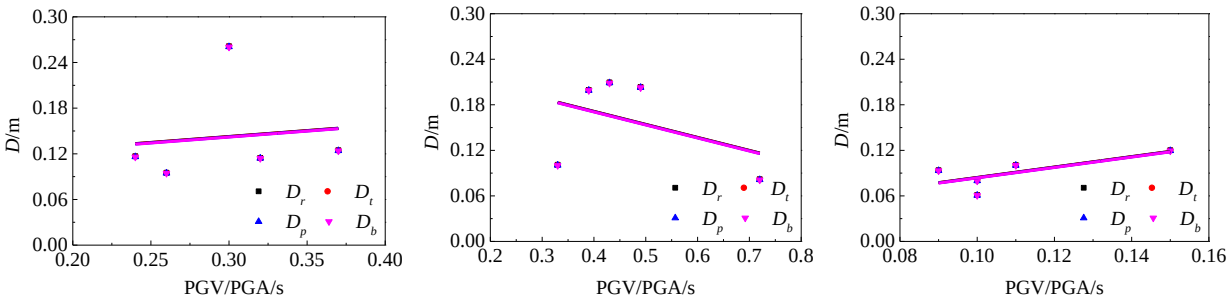

(a) FDP (b) FSP (c) NOP

Fig. 8 PGV/PGA and the lateral dynamic response peak of each layer of the system

4 CONCLUSIONS

(1) In this paper, the HSR-CSII models were established based on FEM (ANSYS and MIDAS). By extracting the time history of the displacement on the top of the bridge pier of the two HSR-CSII models for mutual verification, it was found that the calculation results of the two models were in good agreement, which verified the validity of the models.

(2) Under the transverse excitation of the three groups of ground motions, the envelope diagram and values of the lateral displacement of each layer tend to be

consistent, showing that the FDP is the largest, followed by the FSP, and the NOP is the lowest.

(3) With the increase of PGV/PGA value, the maximum values of longitudinal and lateral displacement of each layer under the action of the FDP, FSP and NOP earthquake basically show an increasing trend.

REFERENCES

Chen L k, Zhang N and Xia H (2016),“Effects of directivity pulse and vertical earthquake on seismic response of high-speed railway bridge”, *Journal of vibration engineering.***29**(04), 704-713.(in Chinese)

Chen L k, Zhang N, Jiang L z and Chen G w (2013),“Analysis of seismic response of directivity pulse-like near-fault ground motion to bridge of high-speed railway”, *Journal of railway engineering society.***180**(09), 40-46. (in Chinese)

China Academy of Railway Sciences (2008),“Summary of Design Principles and Methods of CRTS II Ballastless Track for Beijing-Tianjin Inter-city Railway”, Beijing.

Gou, H., Yang, L., Leng, D., Bao, Y. and Pu, Q. (2018),“Effect of bridge lateral deformation on track geometry of high-speed railway”, *Steel Compos Struct*, **2**(29), 219-229.

Gu, Q., Liu, Y., Guo, W., Li, W., Yu, Z. and Jiang, L. (2019),“A Practical Wheel-Rail Interaction Element for Modeling Vehicle-Track-Bridge Systems”, *Int J Struct Stab Dy*, **19**(02), 1950011.

Jiang L z, Feng Y l, Zhou W b and He B b (2018),“Analysis on natural vibration characteristics of steel-concrete composite truss beam”, *Steel Compos Struct*, **26**(1), 79-87.

Jiang, L., Cao, S. and Wei, B. (2018),“Effects of friction-based fixed bearings on seismic performance of high-speed railway simply supported girder bridges and experimental validation”, *Adv Struct Eng*, **22**(3), 687-701.

Jiang, L., Kang, X., Li, C. and Shao, G. (2019),“Earthquake response of continuous girder bridge for high-speed railway: A shaking table test study”, *Eng Struct*, **180** 249-263.

Jiang, L., Zhang, Y., Feng, Y., Zhou, W. and Tan, Z. (2019),“Dynamic Response Analysis of a Simply Supported Double-Beam System under Successive Moving Loads”, *Applied Sciences*, **9**(10), 2162.

Kang, X., Jiang, L., Bai, Y. and Caprani, C. C. (2017),“Seismic damage evaluation of high-speed railway bridge components under different intensities of earthquake excitations”, *Eng Struct*, **152** 116-128.

Kun, L., Lei, X. and Zeng, S. (2017),“Influence analysis on the effect of rail fastening parameters on the vibration response of track–bridge system”, *Adv Mech Eng*, **9**(8), 2071939371.

Li, X., Liang, L. and Wang, D. (2018),“Vibration and noise characteristics of an elevated box girder paved with different track structures”, *J Sound Vib*, **425** 21-40.

Lizhong Jiang, Yulin Feng, Wangbao Zhou and Binbin He (2019),“Vibration characteristic analysis of high-speed railway simply supported beam bridge-track structure system”, *Steel Compos Struct*, **31**(6), 591-600.

Shao G, Jiang L and N., C. (2014),“Experimental investigations of the seismic performance of bridge piers with rounded rectangular cross-sections”, *Earthq Struct*, **7**(25), 463-484.

Sun, L., Hayashikawa, T., He, X. and Xie, W. (2015),“Influential parameter analysis on vibration responses of rigid-frame viaducts induced by running high-speed trains”, *Int J Steel Struct*, **15**(4), 809-826.

Toyooka A, Ikeda M and Yanagawa H, E. A. (2005),“Effects of track structure on seismic behavior of isolation system bridges”, *Quarterly Report of RTRI*, **46**(4), 238-243.

Zhai Wanming, Zhao Chunfa, Xia He, Xie Youjun, Li Guoqing, Cai Chengbiao, Luo Qiang and Song Xiaolin (2014),“Basic scientific issues on dynamic performance evolution of the high-speed railway infrastructure and its service safety”, *Science China Technological Sciences*(07), 645-660.

Zhang F, Li S, Yan X w and Wang J q (2017),“Effects of near-fault pulse-type ground motions on the seismic responses of a long-span cable-stayed bridge”, *Journal of vibration and shock.* **36**(21), 163-172. (in Chinese)